

Geophysical Research Letters®

RESEARCH LETTER

10.1029/2021GL094872



Key Points:

- We present the first systematic study of ice flow at ice-shelf basal channels. Flow increases with channel size and delays breakthrough
- Linear extrapolation or the Shallow-Shelf Approximation cannot be used to project channel growth, both underestimate channel closure rate
- For ice shelves less than 400 m thick, ice flow does not significantly reduce breakthrough time, potentially influencing iceberg calving

Supporting Information:

Supporting Information may be found in the online version of this article.

Correspondence to:

M. G. Wearing,
mwearing@ed.ac.uk

Citation:

Wearing, M. G., Stevens, L. A., Dutrieux, P., & Kingslake, J. (2021). Ice-shelf basal melt channels stabilized by secondary flow. *Geophysical Research Letters*, 48, e2021GL094872. <https://doi.org/10.1029/2021GL094872>

Received 22 SEP 2021

Accepted 14 OCT 2021

Author Contributions:

Conceptualization: J. Kingslake
Funding acquisition: J. Kingslake
Investigation: L. A. Stevens, P. Dutrieux, J. Kingslake
Methodology: L. A. Stevens
Supervision: J. Kingslake
Writing – review & editing: L. A. Stevens, P. Dutrieux, J. Kingslake

© 2021 The Authors.

This is an open access article under the terms of the [Creative Commons Attribution-NonCommercial License](#), which permits use, distribution and reproduction in any medium, provided the original work is properly cited and is not used for commercial purposes.

Ice-Shelf Basal Melt Channels Stabilized by Secondary Flow

M. G. Wearing¹ , L. A. Stevens^{2,3} , P. Dutrieux^{4,3} , and J. Kingslake³ 

¹School of Geosciences, University of Edinburgh, Edinburgh, UK, ²Department of Earth Sciences, University of Oxford, Oxford, UK, ³Lamont-Doherty Earth Observatory, Columbia University, New York, NY, USA, ⁴British Antarctic Survey, Cambridge, UK

Abstract Ice-shelf basal channels form due to concentrated submarine melting. They are present in many Antarctic ice shelves and can reduce ice-shelf structural integrity, potentially destabilizing ice shelves by full-depth incision. Here, we describe the viscous ice response to a basal channel—secondary flow—which acts perpendicular to the channel axis and is induced by gradients in ice thickness. We use a full-Stokes ice-flow model to systematically assess the transient evolution of a basal channel in the presence of melting. Secondary flow increases with channel size and reduces the rate of channel incision, such that linear extrapolation or the Shallow-Shelf Approximation cannot project future channel evolution. For thick ice shelves (> 600 m) secondary flow potentially stabilizes the channel, but is insufficient to significantly delay breakthrough for thinner ice (< 400 m). Using synthetic data, we assess the impact of secondary flow when inferring basal-channel melt rates from satellite observations.

Plain Language Summary Ice shelves are the floating extensions of ice sheets. At their base, in contact with the ocean, focused melting can lead to the formation of channels incised into the ice. These channels have the potential to incise through the ice shelf completely and thereby destabilize the whole ice shelf. This would lead to a reduction in the resistance provided by the ice shelf, allowing the flow of grounded ice to accelerate and increase contributions to sea-level rise. We use a numerical model to simulate the flow of ice in the vicinity of a channel and demonstrate that the ice flows toward the basal channel, reducing the rate of incision and potentially stabilizing the channel. The rate of ice flow increases as the channel enlarges and, as such, the rate of future channel incision cannot be linearly extrapolated from present observed rates. Basal channels in thick ice shelves (greater than 600 m) can potentially be stabilized by this process. The additional flow induced by the channel means that high-resolution satellite observations of ice thickness and ice velocity are needed in order to accurately infer the submarine melt rate.

1. Introduction

Ice shelves, the floating extensions of ice sheets, form the interface between the ocean and the Antarctic Ice Sheet. Ice shelves melt at their base due to heat supplied by relatively warm ocean waters and buoyant freshwater from subglacial discharge (Jenkins, 1991; Le Brocq et al., 2013; Thoma et al., 2008). Melting is often concentrated in ice-shelf basal channels, where a buoyant meltwater plume entrains relatively warm ambient water, enhancing melting within the channel (Dallaston et al., 2015; Jenkins, 1991). Ice-shelf basal channels, hereafter referred to as basal channels, have been detected in satellite imagery (Alley et al., 2016; Le Brocq et al., 2013), digital surface elevation models (Berger et al., 2017; Chartrand & Howat, 2020; Dutrieux et al., 2013; Howat et al., 2019; Shean et al., 2019), satellite altimetry (Alley et al., 2016; Gourmelen et al., 2017; Wei et al., 2020), ice-penetrating radar (Drews, 2015; Drews et al., 2017; Langley et al., 2014; Rignot & Steffen, 2008; Vaughan et al., 2012), and subshelf cavity observations (Dutrieux et al., 2014, 2016). Basal channels may be initiated upstream of the grounding line (Gladish et al., 2012), by topographic basal highs (Jeoffroy et al., 2018) or focused subglacial drainage (Le Brocq et al., 2013; Wei et al., 2020). Channelized melting may also be initiated by variations in ice-shelf thickness (Dow et al., 2018; Sergienko, 2013).

Modeling and observations indicate that ice-shelf basal melting reduces buttressing to grounded ice (Goldberg et al., 2019; Gudmundsson et al., 2019; Pritchard et al., 2012; Reese et al., 2018). Moreover, concentrated melting in basal channels has been observed to influence the flow and stability of ice shelves. Shear

can increase at a basal channel where the ice is thinner and high strain rates reduce effective viscosity (Drews, 2015; Lhermitte et al., 2020). Surface and basal crevasses have been observed to form aligned with basal channels (Vaughan et al., 2012). Large fractures perpendicular to ice flow can be initiated at basal channels where the ice shelf is thinner (Dow et al., 2018). Furthermore, channels found in ice-shelf shear margins have been implicated in triggering iceberg calving (Alley et al., 2019). Finally, linear extrapolation of current incision rates suggest that basal channels could melt through ice shelves completely, significantly reducing buttressing (Gourmelen et al., 2017; Rignot & Steffen, 2008), although this process is yet to be observed.

In Antarctica, surface meltwater can be produced at low elevations near grounding lines (Kingslake et al., 2017; Lenaerts et al., 2017; Stokes et al., 2019; Trusel et al., 2013). Elongated surface depressions, formed when the ice-shelf surface lowers in response to channelized basal melting, potentially allow water to drain downstream from these spatially restricted ablation zones (Spergel et al., 2021) into areas where the ice shelf is vulnerable to hydro-fracture (Bell et al., 2018; Dow et al., 2018; Kingslake et al., 2017; Lai et al., 2020). Alternatively, they may drain water off the ice-shelf surface and directly into the ocean (Bell et al., 2017).

Ice-shelf basal melting is often inferred using remote-sensing observations of ice surface elevation and velocity (Adusumilli et al., 2018; Berger et al., 2017; Dutrieux et al., 2013; Gourmelen et al., 2017; Paolo et al., 2018; Rignot et al., 2013; Shean et al., 2019). These calculations account for the thinning/thickening of the ice due to horizontal flux divergence/convergence and surface melting/accumulation to determine basal melting/freeze-on, assuming horizontal flow is vertically uniform and the ice shelf is freely floating (Paolo et al., 2018; Pritchard et al., 2012).

Ice-shelf flow is induced by gradients in ice-shelf thickness. The large-scale flow can be calculated using the Shallow-Shelf Approximation (SSA; MacAyeal, 1989), which assumes horizontal gradients in ice thickness are small and horizontal flow is vertically uniform. However, near a basal channel, where gradients in ice thickness are large, the SSA may not apply. The flow of ice induced by a basal channel is referred to as ice-shelf secondary flow (Bassis & Ma, 2015), with primary flow corresponding to the large-scale ice-thickness gradient. Using a 3D full-Stokes ice-flow model, Drews (2015) showed that after concentrated melting channels gradually close due to inflow from the surrounding ice. Furthermore, Drews et al. (2020) showed that the evolution of a basal channel and associated internal stratigraphy is controlled by spatial variations in both basal melting and surface accumulation.

Here, we systematically investigate basal-channel evolution using a full-Stokes ice-flow model. Secondary flow increases with channel size and reduces the growth rate of basal channels. We assess the assumptions used to infer ice-shelf basal melting from remote-sensing observations and discuss the implications of secondary flow for projections of channel incision.

2. Methods

2.1. Full-Stokes Numerical Model

We use the full-Stokes numerical ice-flow model ELMER/Ice (Gagliardini et al., 2013) to simulate the evolution of a basal channel. We consider a 2D vertical plane aligned perpendicular to a basal channel. We assume the domain is advected in the primary flow direction, but do not simulate strain in that direction. This simplification allows us to isolate and explore the physics of secondary flow, while avoiding the computation costs of three-dimensional simulations (Drews, 2015).

The domain is 50 km wide ($x = -25$ to $x = 25$ km) with high horizontal grid resolution (120 m) across the center of the domain and split vertically into 11 evenly spaced layers (see Figure S1 in Supporting Information S1). ELMER/Ice solves the Stokes equations with free upper and lower boundaries that move due to mismatches between buoyancy, vertical velocity and prescribed surface accumulation and basal melting. An idealized melt rate, m , is imposed at the ice-shelf base using a Gaussian function centered at $x = 0$ km with peak melt rate (M_P) and a characteristic width (x_m ; Figure S1c in Supporting Information S1),

$$m = M_P e^{-\frac{x^2}{2x_m^2}}. \quad (1)$$

Surface accumulation, a , is spatially uniform and is either set so that the total accumulation matches the total basal melting (allowing possible steady state),

$$a = \frac{1}{50} \int_{-25}^{25} M_P e^{-\frac{x^2}{2x_m^2}} dx, \quad (2)$$

or a fixed value is prescribed: $a = 1 \text{ m yr}^{-1}$. There is no flow across the lateral boundaries, simulating a laterally confined ice shelf. The ice rheology is specified by Glen's Flow Law, with a uniform rate factor appropriate for ice at -10°C ($A = 3.5 \times 10^{-25} \text{ s}^{-1} \text{ Pa}^{-3}$ Cuffey & Paterson, 2010) and flow-law exponent $n = 3$.

Each simulation is initiated with an ice shelf of uniform thickness, H_0 , and is run for one characteristic time (T_C): the time for cumulative accumulation to equal the ice thickness ($H_0 = aT_C$). Model timesteps are $dt = T_C/500$ (see Section S2 in Supporting Information S1). We vary H_0 , M_P , and x_m between simulations. If the channel incises completely the simulation stops. We perform additional simulations using ELMER/Ice's age solver (Gagliardini et al., 2013) to simulate the internal stratigraphy.

2.2. Inferring Basal Melt Rates From Ice Thickness and Surface Velocity Observations

To mimic satellite observations, we use the surface elevation (h), ice thickness (H), and surface velocity (u_s) calculated in ELMER/Ice (Section 2.1). We test whether the following assumptions used to infer basal melt rates hold in the vicinity of a basal channel: (a) that the horizontal velocity is vertically uniform and therefore equal to the surface velocity; and (b) that the ice shelf is in hydrostatic equilibrium: $H = (1 - \rho_w/\rho)h$, where ρ_w and ρ are the density of seawater and ice, respectively. The inferred basal melt rate, m_{in} , is calculated using the continuity equation:

$$\frac{\partial H}{\partial t} + u_s \frac{\partial H}{\partial x} + H \frac{\partial u_s}{\partial x} = a(x) - m_{in}(x), \quad (3)$$

This approach has the advantage of avoiding additional uncertainties in observations associated with surface mass balance and firn densification. We investigate how the spatial resolution of observations affects the accuracy of the inferred melt rate by varying the resolution of the surface observations through linear interpolation on to grids with 0.25, 0.5, and 1 km spacing.

3. Results

3.1. Evolution of Basal Channels and Secondary Flow

The evolution of a basal channel with $H_0 = 500 \text{ m}$, $M_P = 8 \text{ m yr}^{-1}$ and $x_m = 2.5 \text{ km}$, is shown in Figure 1. Total surface accumulation matches the total basal melting ($a = 1 \text{ m yr}^{-1}$). Initially the height of the basal channel, H_C , increases due to melting (Figure 1a). In response, secondary flow increases with flow directed toward the center of the channel. After 90 years, secondary flow reaches a maximum of approximately 50 m yr^{-1} and the height of the basal channel reaches 99% of its steady-state value. The mean speed continues to adjust, reaching a constant value after approximately 140 years (Figure 1b). A constant geometry is maintained despite continued melt, with secondary flow balancing melting. The steady-state normalized basal channel height \hat{H} is 0.6 (normalized by $H_0 = 500 \text{ m}$). In the absence of secondary flow, the channel would melt through the entire ice shelf in approximately 70 years (Figure 1b).

The age-depth field (Figure 1c) shows isochrones, which are often assumed to be well represented by the internal reflecting horizons imaged with ice-penetrating radar (Drews, 2015; Drews et al., 2017, 2020; Langley et al., 2014; Vaughan et al., 2012). The simulation has been extended to twice the characteristic time ($2T_C = 1000 \text{ year}$) to show isochrones throughout the ice thickness. Isochrones dip down toward the channel and intercept the base where ice has been removed by melting. (Compare with isochrones with higher curvature for $H_0 = 500 \text{ m}$, $M_P = 4 \text{ m yr}^{-1}$ and $x_m = 1 \text{ km}$: Figure S3 in Supporting Information S1).

3.2. The Impact of Ice Thickness, Melt Rate, and Channel Width

For low melt rates ($M_P = 4$ and 8 m yr^{-1} ; Figure 2a), \hat{H} increases monotonically in time, initially approximately linearly then slowing as secondary flow increases until a steady state is reached. Steady-state \hat{H} increases with increasing melt rate, until the basal channel fully breaks through ($M_P = 24$ and 32 m yr^{-1} ;

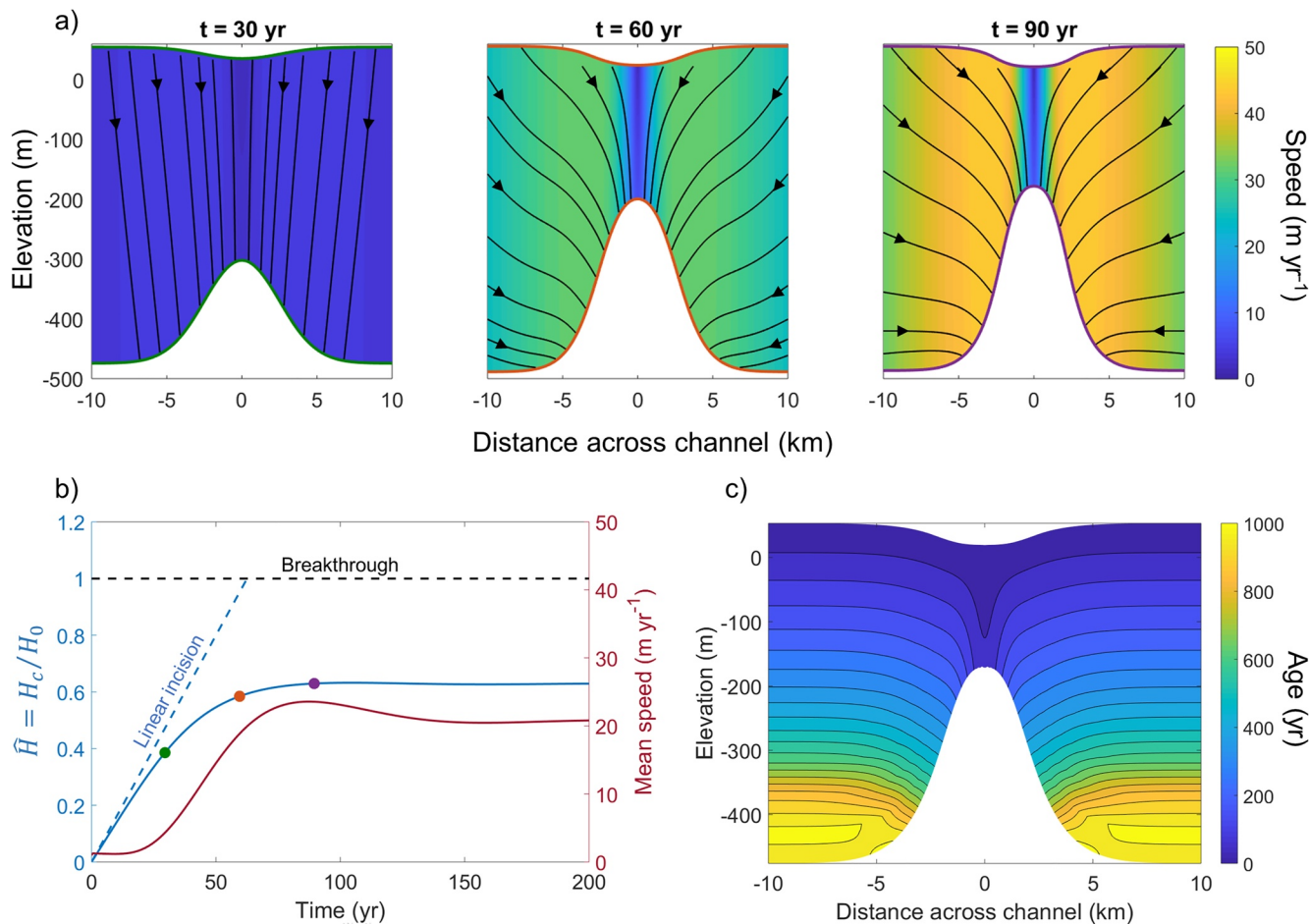


Figure 1. (a) Transient evolution of a basal channel and secondary flow: $H_0 = 500 \text{ m}$, $M_P = 8 \text{ m yr}^{-1}$ and $x_m = 2.5 \text{ km}$. Color scale shows magnitude of secondary flow, and streamlines show direction. (b) Evolution of normalized basal channel height (\hat{H}) (solid blue curve; colored dots correspond to intervals in panel (a)). Linear incision (blue dashed line). $\hat{H} = 1$ indicates breakthrough of basal channel (black dashed line). Mean secondary flow speed (averaged over domain: -25 to 25 km) (red curve). (c) Age-depth field around a basal channel after 1,000 years.

Figure 2a). The timing of breakthrough is delayed (by approximately 6 years or 35%, and 4 years or 30%) in comparison to the linear extrapolation of the melt rate.

Where steady-state \hat{H} is large (>0.8), \hat{H} temporarily grows to exceed its steady-state value. This “overshoot” occurs because secondary flow is dependent on the geometry of the basal channel. The basal channel is initially wider than the steady-state geometry. Horizontal flow narrows the channel, which leads to an increase in vertical velocity and acts to close the channel toward steady state (Figure S5 in Supporting Information S1).

For constant melt rate ($M_P = 16 \text{ m yr}^{-1}$; Figure 2b), thicker shelves (750 and 1,000 m) reach a steady state monotonically. Again, overshoot in \hat{H} occurs for ice shelves with steady-state $\hat{H} > 0.8$. For thinner shelves (250 and 300 m; Figure 2b), secondary flow is insufficient to balance melting; however, there is a delay in breakthrough time (approximately 2.5 years or 16%, and 4 years or 21%, respectively).

Surface accumulation is held constant ($a = 1 \text{ m yr}^{-1}$) and $H_0 = 400 \text{ m}$ with varying M_P in Figure 2c. For $M_P > 8 \text{ m yr}^{-1}$ there is net mass loss and the basal channel breaks through the ice shelf. For high M_P (24 and 32 m yr^{-1}) there is only a small delay in the breakthrough time. However, for lower M_P (12 and 16 m yr^{-1}) there is a substantial increase in the breakthrough time (by a factor of 5 for 12 m yr^{-1}). For ice shelves where there is a net mass gain ($M_P > 8 \text{ m yr}^{-1}$), \hat{H} initially grows as melting incises a channel, but then decreases as secondary flow increases and the ice shelf thickens.

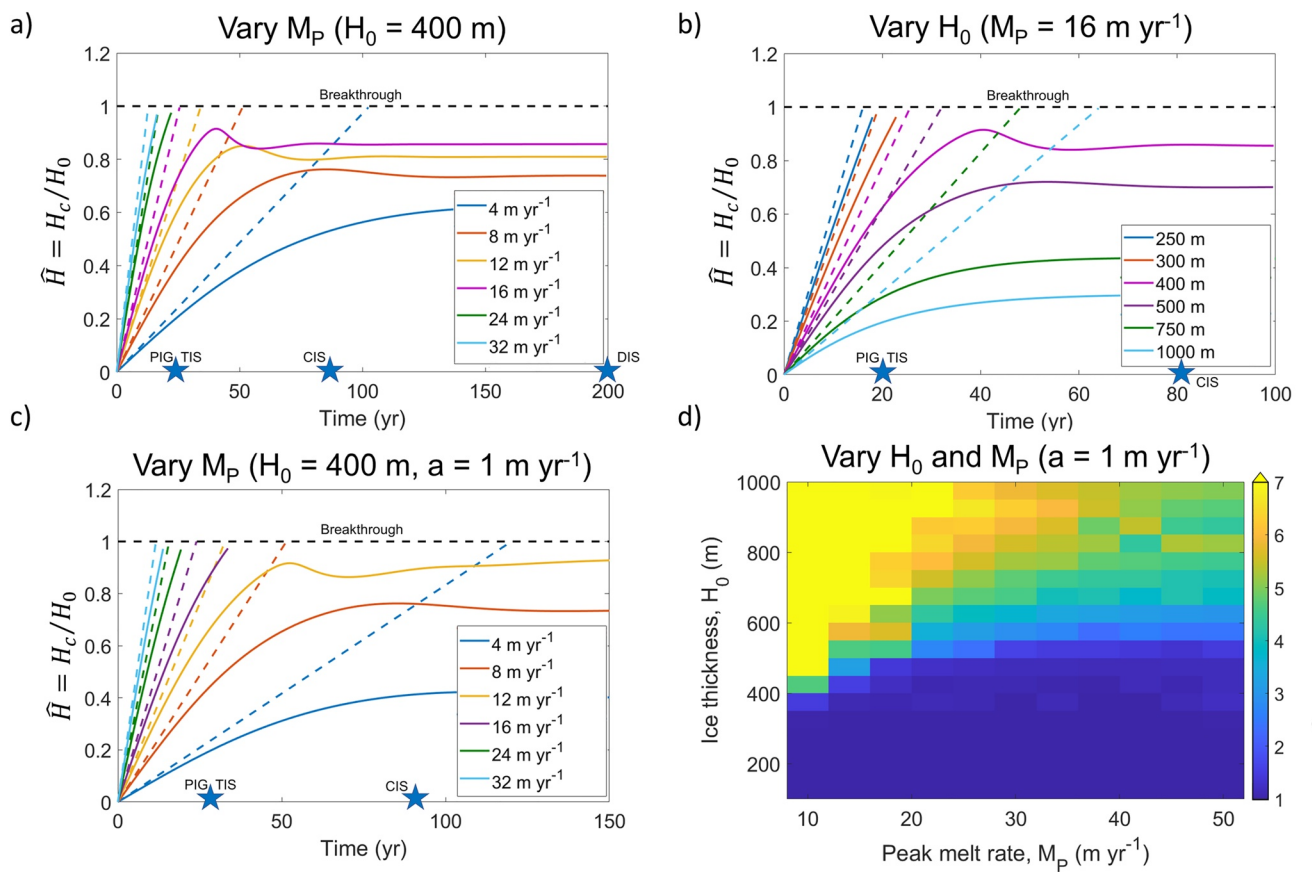


Figure 2. (a)–(c) Evolution of normalized basal channel height (\hat{H}) (solid curves). Dashed black line indicates basal-channel breakthrough ($\hat{H} = 1$) and dashed colored lines denotes linear incision. Stars indicate residence times for: Pine Island Glacier (PIG); Thwaites (TIS); Crosson (CIS) and Dotson (DIS) ice shelves (see Section S6 in Supporting Information S1). (a) and (b) accumulation balances total melt rate. (a) $H_0 = 400$ m and M_P is varied. (b) $M_P = 16 \text{ m yr}^{-1}$ and H_0 is varied. (c) and (d) $a = 1 \text{ m yr}^{-1}$. Accumulation balances melt for $M_P = 8 \text{ m yr}^{-1}$. (c) $H_0 = 400$ m and M_P is varied. (d) Phase space of ice thickness and melt rate depicting breakthrough time with secondary flow normalized by linear incision rate.

In Figures 2a–2c stars indicate the ice-shelf residence time, the time taken for ice to be advected from the grounding line to the calving front, for a selection of Antarctic ice shelves (Figure S6 in Supporting Information S1). For ice shelves with short residence times (< 80 years; Pine Island and Thwaites glaciers), high melt rates ($> 16 \text{ m yr}^{-1}$) and thin ice (< 400 m) are required for basal-channel breakthrough before reaching the calving front. For ice shelves with longer residence times (> 80 years) secondary flow becomes highly significant for melt rates less than 16 m yr^{-1} , with breakthrough time increased to several times the rate expected from linearly extrapolated incision. In these cases, secondary flow prevents channel breakthrough within the residence time.

Figure 2d shows a phase space of ice-shelf thickness and melt rate with the time for basal-channel breakthrough as a multiple of the linearly extrapolated incision rate (e.g., a value of 4 indicates 4 times the linear rate). Accumulation is constant ($a = 1 \text{ m yr}^{-1}$). The largest delays are achieved for thicker ice shelves with smaller melt rates, where secondary flow can be sustained without thinning the ice rapidly. For thin ice shelves ($H_0 < 400$ m), only small delays in breakthrough time are possible as the ice shelf is not thick enough to produce substantial secondary flow. For thicker ice shelves, $H_0 > 600$ m, the breakthrough time is substantially increased to over four times the linear incision rate. In all cases in Figure 2d ($10 \leq M_P \leq 50 \text{ m yr}^{-1}$) there is net mass loss and eventually channel breakthrough. Melting balances accumulation for $M_P = 8 \text{ m yr}^{-1}$, and hence the breakthrough time approaches infinity, for $H_0 > 400$ m, toward the left vertical boundary.

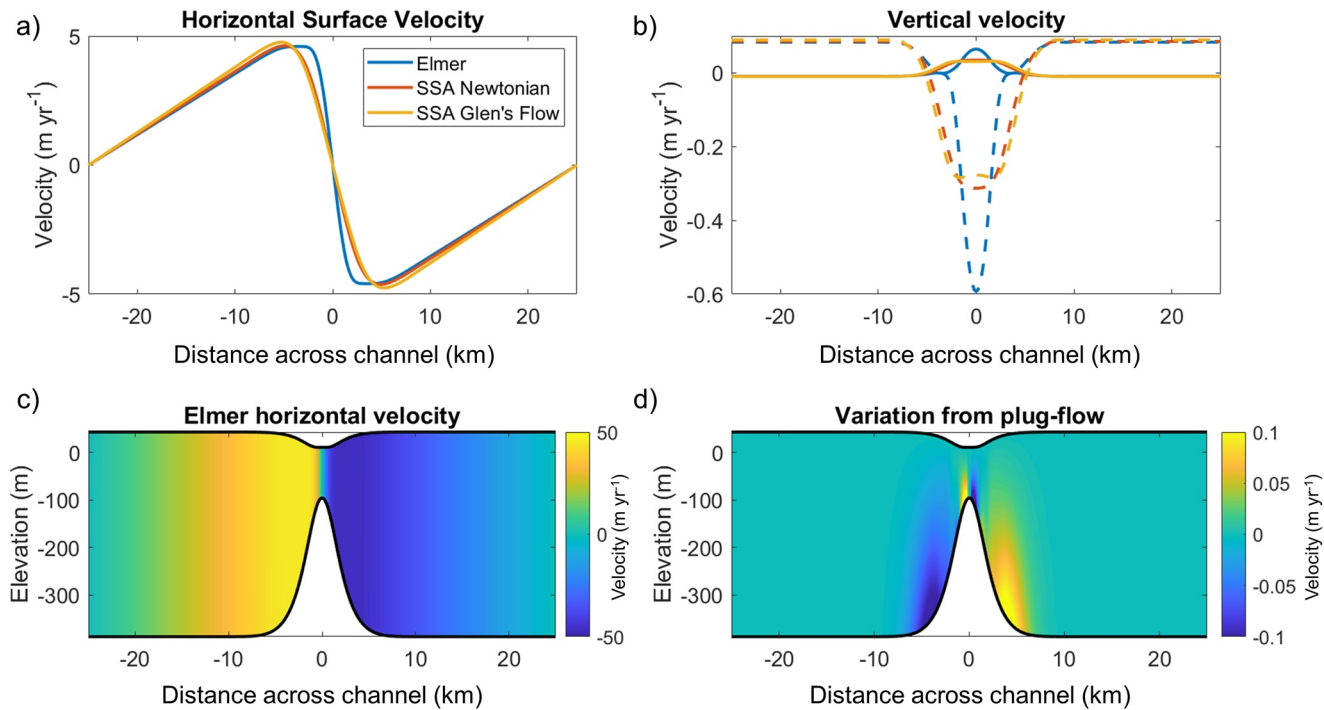


Figure 3. (a and b) Comparing velocities from the full-Stokes ELMER/Ice simulations and the SSA, for a prescribed basal channel geometry ($H_C = 180$ m, $H_0 = 400$ m; Figure S8 in Supporting Information S1), with no melting or accumulation. (a) Horizontal velocity at the ice surface. (b) Vertical velocity at the ice surface (solid lines) and base (dashed lines). (c and d) Steady-state ELMER/Ice simulation with $H_0 = 400$ m, $M_P = 8 \text{ m yr}^{-1}$ and $x_m = 2.5$ km ($H_C \approx 300$ m, $H_0 = 400$ m). (c) Horizontal velocity. (d) Vertical variation in horizontal flow from surface velocity.

All simulations in Figure 2 feature melting with characteristic width $x_m = 2.5$ km. Figures S7c and S7f in Supporting Information S1 show the effect of changing x_m on the evolution of \hat{H} . In all cases decreasing x_m , but maintaining M_P , leads to a decrease in \hat{H} , as narrower channels induce a larger vertical flow.

3.3. Comparing Numerical Model and Shallow-Shelf Approximation

To compare the SSA and full-Stokes model, we consider the instantaneous velocity in the absence of accumulation or melting (Section S8 in Supporting Information S1; Figure 3). The SSA viscosity parameters for Newtonian and Glen's Flow Law rheologies are uniform across the domain and are chosen to match the peak magnitude in horizontal surface velocity from ELMER/Ice (Figure 3a). The SSA vertical velocities are approximately half the magnitude of the ELMER/Ice velocity at $x = 0$ km, and larger than the ELMER/Ice velocities either side of the central peak ($x = \pm 1.5$ to $x = \pm 5$ km; Figure 3b).

While the SSA disagrees significantly with the full-Stokes ELMER/Ice simulation, a separate question is whether there is a large deviation from vertically uniform flow. This question is important because remote-sensing estimates of ice-shelf basal melting assume horizontal flow is vertically uniform. A steady-state ELMER/Ice simulation ($H_0 = 400$ m, $M_P = 8 \text{ m yr}^{-1}$, $x_m = 2.5$ km and $a = 1 \text{ m yr}^{-1}$) shows that horizontal flow varies by less than 1% with depth (Figure 3d), with the most significant variation aligned with the highest curvature of channel geometry (onset and peak of channel). The presence of horizontal and vertical shear (Figure S9 in Supporting Information S1) emphasizes the fact that despite near uniform horizontal flow, higher-order stresses, neglected in SSA, are important here.

3.4. Inferring Basal Melt From Remote-Sensing Observations

Using H allows the mismatch between the inferred and imposed melt rate due to spatial resolution to be assessed without additional impacts from non-hydrostatic effects (Figures 4a and 4b). Spatial resolution of 250 m leads to a slight underestimate of the peak melt rate of 2.5%, and this increases to 10% and 30%

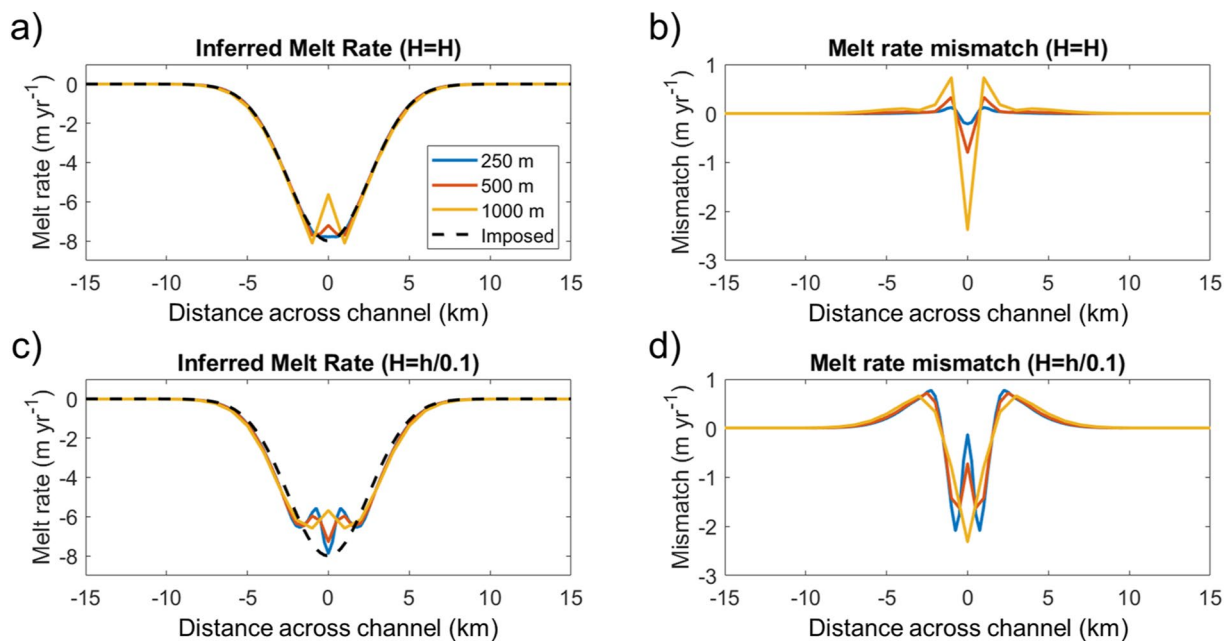


Figure 4. Inferred (colored curves) and imposed (dashed black curve) melt rates for $H_0 = 400$ m and $M_P = 8 \text{ m yr}^{-1}$ with steady-state \hat{H} ($\frac{dH}{dx} < 0.1 \text{ m yr}^{-1}$) (see Figure 3c for thickness profile). Different colored curves correspond to resolution of synthetic data. (a) Inferred melt rate using ice thickness H . (b) The mismatch between inferred and imposed melt rate in (a). Panels (c), (d) same as (a), (b) but the surface elevation h is used to determine ice thickness assuming hydrostatic equilibrium.

when the resolution is reduced to 500 m and 1 km. At the channel margins ($x = \pm 1$ to $x = \pm 4$ km) the melt rate is overestimated. These mismatches result from linear interpolation of ice-shelf thickness and surface expression of secondary flow, with the exact pattern and magnitude of the mismatch depending on the ice-shelf thickness and the channel geometry (Figure S10 in Supporting Information S1). The largest errors result from the interpolation of secondary flow across the basal channel (Figure S11 in Supporting Information S1) where there is the largest gradient in horizontal velocity (Figure 3a).

The mismatch increases to 25% when the incorrect assumption of hydrostatic equilibrium is used to determine H (Figures 4c and 4d; 250-m resolution). Melt rate is underestimated at the channel center, but overestimated in the flanks ($|x| > 2.5$ km). The magnitude of the mismatch varies with H_0 and M_P (Figure S12 in Supporting Information S1). In general, for smaller \hat{H} , the mismatch is reduced because the ice is closer to hydrostatic equilibrium. Prior to reaching steady state, the mismatch increases as the channel grows (Figure S12 in Supporting Information S1). The largest errors are aligned with the channel walls, where bridging stresses become significant and inaccuracies in the ice-thickness gradient contribute the most to the mismatch (Figure S13 in Supporting Information S1). Despite these spatial patterns of large mismatch, integrated over the whole domain, the mismatch in total melting is less than 1%.

4. Discussion

Secondary flow counteracts the growth of ice-shelf basal channels formed by concentrated submarine melting. This not only allows basal channels to close once melting has stopped (Drews, 2015), but also reduces the growth rate of channels as they enlarge. Secondary flow is dependent on the basal-channel geometry and increases for larger channels, potentially stabilizing a basal channel despite continued melting.

Where an ice shelf experiences net mass balance, secondary flow can prevent the complete incision of a basal channel through the ice shelf. Where ice shelves experience net mass loss, secondary flow extends the time until basal-channel breakthrough, up to multiple times the rate calculated by linear extrapolation of incision rates. The exact delay depends on the net mass balance, the geometry of the ice shelf and the basal channel. Therefore, secondary flow should be accounted for when estimating future growth of basal

channels and, in turn, ice-shelf stability. In the case of a basal channel identified in the Dotson Ice Shelf (Gourmelen et al., 2017), secondary flow may increase the time until channel breakthrough by 30% (8 years; Figure S14 in Supporting Information S1).

For the fastest flowing ice shelves (e.g., Pine Island Glacier and Thwaites Glacier), secondary flow can prevent the complete breakthrough of a basal channel within the ice-shelf residence time (i.e., for $H_0 > 400$ m and $M_P = 16 \text{ m yr}^{-1}$) or significantly increase the time until breakthrough for higher melt rates. For the majority of ice shelves with residence times greater than 200 years (Figure S6 in Supporting Information S1), secondary flow has the potential to prevent breakthrough of basal channels, with the exact results dependent on the magnitude of melting, ice-shelf thickness and net mass balance.

Ice-shelf secondary flow is encoded into the age-depth structure of the ice shelf (Figure 1c). Isochrones imaged with ice-penetrating radar have the potential to reveal the history of basal melting and surface accumulation (Catania et al., 2006, 2010; Drews et al., 2020; Wearing & Kingslake, 2019). Future work could develop the potential to invert basal-melt history from isochrone stratigraphy.

Our assessment considers a basal channel aligned in the primary flow direction with no additional extensional stress acting across the channel. However, if a channel is aligned perpendicular to flow, we might expect additional extensional stresses across it to reduce secondary flow and, if large enough, ultimately prevent it (Bassis & Ma, 2015). In contrast, compression across the channel would enhance, channel closure. Our idealized model neglects extension in the primary flow direction. To first order, this would lead to ice-shelf thinning inside and outside of the channel, proportional to the local ice thickness, decreasing the gradient in ice-shelf thickness and in turn reducing secondary flow.

Ice fracturing may become important as the channel approaches breakthrough. Our results show extensional and shear stresses that are less than the critical stress required for fracturing ($\approx 100 \text{ kPa}$; Vaughan, 1993; Figure S4 in Supporting Information S1). However, if the basal channel geometry is instantaneously imposed, high extensional stresses, capable of fracturing, are found above the apex of the channel and at the surface in the channel flanks (Vaughan et al., 2012). Channels aligned perpendicular to the primary flow may experience additional extensional stress due to the large-scale flow of the ice shelf, which can induce concentrated ductile deformation and potential crevassing (Bassis & Ma, 2015). The fracture reported by Dow et al. (2018) on the Nansen Ice Shelf occurred perpendicular to the channel axis and primary flow direction, with the thinner ice acting as the initiation site for fracture. Similar processes likely occur in ice-shelf shear margins (Alley et al., 2019). Although stresses generated by along-flow basal channels may not trigger fracturing on their own, the presence of thinner ice at a basal channel may allow full-depth penetration of fractures induced by the large-scale stress regime. This may be particularly important where the ice is thin ($< 400 \text{ m}$) and secondary flow is insufficient to delay incision, potentially triggering the iceberg calving. Channelized basal melting has been implicated in the increase in ice damage in the shear margins of Pine Island Ice Shelf (Lhermitte et al., 2020), which consequently led to large calving events and ice acceleration (Joughin et al., 2021).

Despite the small variation in horizontal flow with depth (Figure 3d), secondary flow at a basal channel cannot be determined using the SSA. This is because large ice-thickness gradients around a basal channel induce higher-order stresses that are neglected in the SSA. However, ice-surface velocity and thickness data that are spatially well-resolved ($\leq 250\text{-m}$) can be used to infer the basal melt rate, assuming vertically uniform velocity (Equation 3), with errors of less than 5%. This accuracy decreases significantly when the ice thickness is determined from surface elevation assuming hydrostatic equilibrium. The mismatch increases as basal channels enlarge and ice is held out of hydrostatic equilibrium. The accuracy decreases further as the spatial resolution of the data is reduced, which effectively smooths gradients in the horizontal velocity and ice-shelf thickness across the channel, with the largest errors resulting from linear interpolation of secondary flow. This is important for accurately resolving the spatial patterns of melting, but the integrated effect on total melt rate is small.

Using synthetic data has allowed us to assess the impacts of data resolution and non-hydrostatic ice on estimates of basal melting. However, when using remote-sensing data, additional uncertainties are introduced in the form of spatial and temporal changes in surface mass balance and firn density. These processes impact calculations of ice-shelf surface elevation change and ice-shelf thickness under the hydrostatic

assumption. Future work could include these processes to provide a comprehensive assessment of the uncertainties associated with inferring melt rates from remote-sensing observations.

We have imposed a simple melt rate with a Gaussian profile, further complexity may arise through dependence on depth, basal slope, along-flow position, ocean heat content, plume entrainment rates, Coriolis effects and ice-shelf cavity circulation (Dallaston et al., 2015; Dutrieux et al., 2013; Jenkins, 1991; Millgate et al., 2013; Sergienko, 2013; Slater & Straneo, 2018). In some simulations, we set total surface accumulation equal to total basal melting, so that a steady state can be achieved. This is unrealistic for large melt rates ($M_P \geq 25 \text{ m yr}^{-1}$, $x_m = 2.5 \text{ km}$) when accumulation is larger than observed on Antarctic ice shelves ($a \geq 2.5 \text{ m yr}^{-1}$). However, increasing the width of the domain would act in a similar manner to increased accumulation rates. Similar limitations apply to calculating delayed breakthrough (Figure 2d), where the results would vary quantitatively with the width of the embayment and the accumulation rate. Furthermore, future work could quantify the impact of varying ice rheology parameters A and n on the stabilizing effect of secondary flow.

5. Conclusion

Ice-shelf secondary flow acts to counter the growth of basal-melt channels. The magnitude of secondary flow is dependent on the channel geometry and increases for larger basal channels. This delays the time for a channel to completely incise through an ice shelf and, depending on the net mass balance, can stabilize a basal channel in the presence of continuous melting.

Close to ice-shelf calving fronts, where the ice is thin (< 400 m), secondary flow cannot significantly delay basal-channel breakthrough. Here, basal channels may act as the initiation point for fracturing leading to iceberg calving. However, further upstream in areas of thicker ice, secondary flow can substantially reduce channel incision.

High resolution ($\leq 250\text{-m}$) observations of ice-shelf thickness and surface velocity can be used to infer basal-melt patterns with errors of less than 5%. However, this accuracy is dependent on correctly determining ice-shelf thickness.

Despite only small variations in horizontal velocity with depth, the SSA is unable to accurately predict secondary flow because higher-order stresses become important near channels where the ice thickness gradient is large. Furthermore, linear extrapolation of a channel incision rate or the SSA is unable to accurately determine the timing of channel breakthrough. It is necessary to consider the dynamics of secondary flow to accurately predict the future growth of basal channels and their effect on ice-shelf stability and the longevity of ice shelves.

Data Availability Statement

ELMER/Ice program files and model results corresponding to simulations presented in Figure 1 is available at: <https://hdl.handle.net/10283/3893>.

Acknowledgments

Support to M. G. Wearing and J. Kingslake was provided by NSF grant number 1743310. Support to L. A. Stevens was provided by a Lamont-Doherty Earth Observatory Postdoctoral Fellowship. The authors thank Dan Goldberg, Noel Gourmelen, Paul Holland and Richard Hindmarsh for useful discussions related to this work. Furthermore, the authors would also like to thank the two reviewers; Reinhard Drews and Lizz Ultee, along with the editor for their feedback and comments, which greatly improved the manuscript.

References

- Adusumilli, S., Fricker, H. A., Siegfried, M. R., Padman, L., Paolo, F. S., & Ligtenberg, S. R. (2018). Variable basal melt rates of Antarctic Peninsula Ice Shelves, 1994–2016. *Geophysical Research Letters*, 45(9), 4086–4095. <https://doi.org/10.1002/2017GL076652>
- Alley, K. E., Scambos, T. A., Alley, R. B., & Holschuh, N. (2019). Troughs developed in ice-stream shear margins precondition ice shelves for ocean-driven breakup. *Science Advances*, 5(10), eaax2215. <https://doi.org/10.1126/sciadv.aax2215>
- Alley, K. E., Scambos, T. A., Siegfried, M. R., & Fricker, H. A. (2016). Impacts of warm water on Antarctic ice shelf stability through basal channel formation. *Nature Geoscience*, 9(4), 290–293. <https://doi.org/10.1038/ngeo2675>
- Bassis, J., & Ma, Y. (2015). Evolution of basal crevasses links ice shelf stability to ocean forcing. *Earth and Planetary Science Letters*, 409, 203–211. <https://doi.org/10.1016/j.epsl.2014.11.003>
- Bell, R. E., Banwell, A. F., Trusel, L. D., & Kingslake, J. (2018). Antarctic surface hydrology and impacts on ice-sheet mass balance. *Nature Climate Change*, 8(12), 1044–1052. <https://doi.org/10.1038/s41558-018-0326-3>
- Bell, R. E., Chu, W., Kingslake, J., Das, I., Tedesco, M., Tinto, K. J., et al. (2017). Antarctic ice shelf potentially stabilized by export of meltwater in surface river. *Nature*, 544(7650), 344–348. <https://doi.org/10.1038/nature22048>
- Berger, S., Drews, R., Helm, V., Sun, S., & Pattyn, F. (2017). Detecting high spatial variability of ice shelf basal mass balance, Roi Baudouin Ice Shelf, Antarctica. *The Cryosphere*, 11(6), 2675–2690. <https://doi.org/10.5194/tc-11-2675-2017>

- Catania, G., Hulbe, C., & Conway, H. (2010). Grounding-line basal melt rates determined using radar-derived internal stratigraphy. *Journal of Glaciology*, 56(197), 545–554. <https://doi.org/10.3189/002214310792447842>
- Catania, G., Scambos, T. A., Conway, H., & Raymond, C. F. (2006). Sequential stagnation of Kamb Ice Stream, West Antarctica. *Geophysical Research Letters*, 33(14), L14502. <https://doi.org/10.1029/2006GL026430>
- Chartrand, A. M., & Howat, I. M. (2020). Basal channel evolution on the Getz Ice Shelf, West Antarctica. *Journal of Geophysical Research: Earth Surface*, 125(9), 1–18. <https://doi.org/10.1029/2019JF005293>
- Cuffey, K. M., & Paterson, W. S. B. (2010). *The physics of glaciers* (4th ed.). Elsevier.
- Dallaston, M. C., Hewitt, I. J., & Wells, A. J. (2015). Channelization of plumes beneath ice shelves. *Journal of Fluid Mechanics*, 785, 109–134. <https://doi.org/10.1017/jfm.2015.609>
- Dow, C. F., Lee, W. S., Greenbaum, J. S., Greene, C. A., Blankenship, D. D., Poinar, K., et al. (2018). Basal channels drive active surface hydrology and transverse ice shelf fracture. *Science Advances*, 4(6), eaao7212. <https://doi.org/10.1126/sciadv.aao7212>
- Drews, R. (2015). Evolution of ice-shelf channels in Antarctic ice shelves. *The Cryosphere*, 9(3), 1169–1181. <https://doi.org/10.5194/tc-9-1169-2015>
- Drews, R., Pattyn, F., Hewitt, I. J., Ng, F. S. L., Berger, S., Matsuoka, K., et al. (2017). Actively evolving subglacial conduits and eskers initiate ice shelf channels at an Antarctic grounding line. *Nature Communications*, 8, 15228. <https://doi.org/10.1038/ncomms15228>
- Drews, R., Schannwell, C., Ehlers, T. A., Gladstone, R., Pattyn, F., & Matsuoka, K. (2020). Atmospheric and oceanographic signatures in the Ice Shelf Channel Morphology of Roi Baudouin Ice Shelf, East Antarctica, inferred from radar data. *Journal of Geophysical Research: Earth Surface*, 125(7), e2020JF005587. <https://doi.org/10.1029/2020JF005587>
- Dutrieux, P., Jenkins, A., & Nicholls, K. W. (2016). Ice-shelf basal morphology from an upward-looking multibeam system deployed from an autonomous underwater vehicle. *Geological Society, London, Memoirs*, 46(1), 219–220. <https://doi.org/10.1144/M46.79>
- Dutrieux, P., Stewart, C., Jenkins, A., Nicholls, K. W., Corr, H. F. J., Rignot, E., & Steffen, K. (2014). Basal terraces on melting ice shelves. *Geophysical Research Letters*, 41, 5506–5513. <https://doi.org/10.1002/2014GL060618>
- Dutrieux, P., Vaughan, D. G., Corr, H. F. J., Jenkins, A., Holland, P. R., Joughin, I., & Fleming, A. H. (2013). Pine Island glacier ice shelf melt distributed at kilometre scales. *The Cryosphere*, 7(5), 1543–1555. <https://doi.org/10.5194/tc-7-1543-2013>
- Gagliardini, O., Zwinger, T., Gillet-Chaulet, F., Durand, G., Favier, L., de Fleurian, B., et al. (2013). Capabilities and performance of Elmer/Ice, a new-generation ice sheet model. *Geoscientific Model Development*, 6(4), 1299–1318. <https://doi.org/10.5194/gmd-6-1299-2013>
- Gladish, C. V., Holland, D. M., Holland, P. R., & Price, S. F. (2012). Ice-shelf basal channels in a coupled ice/ocean model. *Journal of Glaciology*, 58(212), 1227–1244. <https://doi.org/10.3189/2012JoG12J003>
- Goldberg, D. N., Gourmelen, N., Kimura, S., Millan, R., & Snow, K. (2019). How accurately should we model ice shelf melt rates? *Geophysical Research Letters*, 46(1), 189–199. <https://doi.org/10.1029/2018GL080383>
- Gourmelen, N., Goldberg, D. N., Snow, K., Henley, S. F., Bingham, R. G., Kimura, S., et al. (2017). Channelized melting drives thinning under a rapidly melting Antarctic Ice Shelf. *Geophysical Research Letters*, 44(19), 9796–9804. <https://doi.org/10.1002/2017GL074929>
- Gudmundsson, G. H., Paolo, F. S., Adusumilli, S., & Fricker, H. A. (2019). Instantaneous Antarctic ice sheet mass loss driven by thinning ice shelves. *Geophysical Research Letters*, 46(23), 13903–13909. <https://doi.org/10.1029/2019GL085027>
- Howat, I. M., Porter, C., Smith, B. E., Noh, M.-J., & Morin, P. (2019). The reference elevation model of Antarctica. *The Cryosphere*, 13(2), 665–674. <https://doi.org/10.5194/tc-13-665-2019>
- Jenkins, A. (1991). A one-dimensional model of ice shelf-ocean interaction. *Journal of Geophysical Research*, 96(C11), 20671. <https://doi.org/10.1029/91JC01842>
- Jeoffry, H., Ross, N., Le Brocq, A., Graham, A. G., Li, J., Gogineni, P., et al. (2018). Hard rock landforms generate 130 km ice shelf channels through water focusing in basal corrugations. *Nature Communications*, 9(1), 4576. <https://doi.org/10.1038/s41467-018-06679-z>
- Joughin, I., Shapero, D., Smith, B., Dutrieux, P., & Barham, M. (2021). Ice-shelf retreat drives recent Pine Island Glacier speedup. *Science Advances*, 7(24), eabg3080. <https://doi.org/10.1126/sciadv.abg3080>
- Kingslake, J., Ely, J. C., Das, I., & Bell, R. E. (2017). Widespread movement of meltwater onto and across Antarctic ice shelves. *Nature*, 544(7650), 349–352. <https://doi.org/10.1038/nature22049>
- Lai, C.-Y., Kingslake, J., Wearing, M. G., Chen, P.-H. C., Gentine, P., Li, H., et al. (2020). Vulnerability of Antarctica's ice shelves to meltwater-driven fracture. *Nature*, 584(7822), 574–578. <https://doi.org/10.1038/s41586-020-2627-8>
- Langley, K., von Deschwendt, A., Kohler, J., Sinisalo, A., Matsuoka, K., Hattermann, T., et al. (2014). Complex network of channels beneath an Antarctic ice shelf. *Geophysical Research Letters*, 41(4), 1209–1215. <https://doi.org/10.1002/2013GL058947>
- Le Brocq, A. M., Ross, N., Griggs, J. A., Bingham, R. G., Corr, H. F. J., Ferraccioli, F., et al. (2013). Evidence from ice shelves for channelized meltwater flow beneath the Antarctic Ice Sheet. *Nature Geoscience*, 6(11), 945–948. <https://doi.org/10.1038/ngeo1977>
- Lenaerts, J. T. M., Lhermitte, S., Drews, R., Ligtenberg, S. R. M., Berger, S., Helm, V., et al. (2017). Meltwater produced by wind-albedo interaction stored in an East Antarctic ice shelf. *Nature Climate Change*, 7(1), 58–62. <https://doi.org/10.1038/nclimate3180>
- Lhermitte, S., Sun, S., Shuman, C., Wouters, B., Pattyn, F., Wuite, J., et al. (2020). Damage accelerates ice shelf instability and mass loss in Amundsen Sea Embayment. *Proceedings of the National Academy of Sciences*, 117(40), 24735–24741. <https://doi.org/10.1073/pnas.1912890117>
- MacAyeal, D. R. (1989). Large-scale ice flow over a viscous basal sediment: Theory and application to ice stream B, Antarctica. *Journal of Geophysical Research*, 94(B4), 4071–4087. <https://doi.org/10.1029/JB094iB04p04071>
- Millgate, T., Holland, P. R., Jenkins, A., & Johnson, H. L. (2013). The effect of basal channels on oceanic ice-shelf melting. *Journal of Geophysical Research: Oceans*, 118(12), 6951–6964. <https://doi.org/10.1002/2013JC009402>
- Paolo, F. S., Padman, L., Fricker, H. A., Adusumilli, S., Howard, S., & Siegfried, M. R. (2018). Response of Pacific-sector Antarctic ice shelves to the El Niño/Southern Oscillation. *Nature Geoscience*, 11, 121–126. <https://doi.org/10.1038/s41561-017-0033-0>
- Pritchard, H. D., Ligtenberg, S. R. M., Fricker, H. A., Vaughan, D. G., van den Broeke, M. R., & Padman, L. (2012). Antarctic ice-sheet loss driven by basal melting of ice shelves. *Nature*, 484(7395), 502–505. <https://doi.org/10.1038/nature10968>
- Reese, R., Gudmundsson, G. H., Levermann, A., & Winkelmann, R. (2018). The far reach of ice-shelf thinning in Antarctica. *Nature Climate Change*, 8(1), 53–57. <https://doi.org/10.1038/s41558-017-0020-x>
- Rignot, E., Jacobs, S., Mouginot, J., & Scheuchl, B. (2013). Ice-shelf melting around Antarctica. *Science*, 341(6143), 266–270. <https://doi.org/10.1126/science.1235798>
- Rignot, E., & Steffen, K. (2008). Channelized bottom melting and stability of floating ice shelves. *Geophysical Research Letters*, 35(2), L02503. <https://doi.org/10.1029/2007GL031765>
- Sergienko, O. V. (2013). Basal channels on ice shelves. *Journal of Geophysical Research: Earth Surface*, 118(3), 1342–1355. <https://doi.org/10.1002/jgrf.20105>

- Shean, D. E., Joughin, I. R., Dutrieux, P., Smith, B. E., & Berthier, E. (2019). Ice shelf basal melt rates from a high-resolution digital elevation model (DEM) record for Pine Island Glacier, Antarctica. *The Cryosphere*, 13(10), 2633–2656. <https://doi.org/10.5194/tc-13-2633-2019>
- Slater, D. A., Straneo, F., Das, S. B., Richards, C. G., Wagner, T. J. W., & Nienow, P. W. (2018). Localized plumes drive front-wide ocean melting of a Greenlandic Tidewater Glacier. *Geophysical Research Letters*, 45, 350–358. <https://doi.org/10.1029/2018GL080763>
- Spergel, J. J., Kingslake, J., Creyts, T., van Wessem, M., & Fricker, H. A. (2021). Surface meltwater drainage and ponding on Amery Ice Shelf, East Antarctica, 1973–2019. *Journal of Glaciology*, 1–14. <https://doi.org/10.1017/jog.2021.46>
- Stokes, C. R., Sanderson, J. E., Miles, B. W. J., Jamieson, S. S. R., & Leeson, A. A. (2019). Widespread distribution of supraglacial lakes around the margin of the East Antarctic Ice Sheet. *Scientific Reports*, 9(1), 13823. <https://doi.org/10.1038/s41598-019-50343-5>
- Thoma, M., Jenkins, A., Holland, D., & Jacobs, S. (2008). Modelling circumpolar deep water intrusions on the Amundsen Sea continental shelf, Antarctica. *Geophysical Research Letters*, 35(18), 1–6. <https://doi.org/10.1029/2008GL034939>
- Trusel, L. D., Frey, K. E., Das, S. B., Munneke, P. K., & Van Den Broek, M. R. (2013). Satellite-based estimates of Antarctic surface meltwater fluxes. *Geophysical Research Letters*, 40(23), 6148–6153. <https://doi.org/10.1002/2013GL058138>
- Vaughan, D. G. (1993). Relating the occurrence of crevasses to surface strain rates. *Journal of Glaciology*, 39(132), 255–266. <https://doi.org/10.3189/S0022143000015926>
- Vaughan, D. G., Corr, H. F. J., Bindschadler, R. A., Dutrieux, P., Gudmundsson, G. H., Jenkins, A., et al. (2012). Subglacial melt channels and fracture in the floating part of Pine Island Glacier, Antarctica. *Journal of Geophysical Research*, 117(F3). <https://doi.org/10.1029/2012JF002360>
- Wearing, M. G., & Kingslake, J. (2019). Holocene Formation of Henry Ice Rise, West Antarctica, Inferred From Ice-Penetrating Radar. *Journal of Geophysical Research: Earth Surface*, 124(8), 2224–2240. <https://doi.org/10.1029/2018JF004988>
- Wei, W., Blankenship, D. D., Greenbaum, J. S., Gourmelen, N., Dow, C. F., Richter, T. G., et al. (2020). Getz Ice Shelf melt enhanced by freshwater discharge from beneath the West Antarctic Ice Sheet. *The Cryosphere*, 14(4), 1399–1408. <https://doi.org/10.5194/tc-14-1399-2020>